Desalination and Water Treatment
www.deswater.com
doi: 10.1080/19443994.2015.1069219

57 (2016) 15073–15082
July

Taylor & Francis
Taylor & Francis Group

Pb(II)-imprinted chitosan beads to enhance the adsorption property and selectivity: characterization, kinetics, and thermodynamics

Yingjun Jing*, Nana Yin, Xueqing Yu

School of Chemical Engineering and Technology, Hebei University of Technology, Tianjin 300130, China, Tel. +86 22 60200444; emails: jingyingjun@hebut.edu.cn (Y. Jing), nanayin08@hotmail.com (N. Yin), Tel. +86 22 60204281; email: tcyu999@126.com (X. Yu)

Received 18 November 2014; Accepted 27 June 2015

ABSTRACT

An effective and selective ion-imprinted biosorbent was prepared from chitosan, using Pb(II) ions as templates and ethylene glycol diglycidyl ether as the crosslinker. The resultant Pb(II)-imprinted chitosan beads (Pb-ICB) were characterized by Fourier transform infrared spectroscopy, scanning electron microscopy, X-ray diffraction, and thermogravimetric analysis. The adsorption property and selectivity of Pb-ICB were evaluated for the adsorption of Pb(II). The results showed that Pb-ICB had more cavities, but lower crystallinity and thermal stability than non-imprinted chitosan beads (NICB). Much higher adsorption capacity in the single metal system and better selectivity in the binary metal system for the adsorption Pb(II) were achieved with Pb-ICB than NICB. The maximum adsorption capacity of Pb (II) on Pb-ICB reached 177.62 mg/g. The kinetic and isothermal analyzes showed that the adsorption process of Pb(II) onto Pb-ICB well-fitted pseudo-second-order kinetic and Langmuir isotherm models. The thermodynamic analysis revealed that the adsorption of Pb(II) onto Pb-ICB was a spontaneous and endothermic process. Furthermore, Pb-ICB showed good reusability within five cycles of adsorption–desorption.

Keywords: Ion-imprinting; Adsorption; Kinetics; Thermodynamics; Selectivity

1. Introduction

Lead is one of the earliest refined heavy metals in the world and has been extensively used in numerous fields such as battery [1], paint [2], ammunition [3], construction [4], and electrical industries [5]. However, lead pollution emerged recently due to the discharge of industrial wastewater without proper treatments, which can cause severe damage to the natural environment and human health. Therefore, it is imperative to remove lead ions from wastewater before discharge. Currently, wastewater is conventionally disposed by several methods, including ion exchange, chemical precipitation, adsorption, and membrane process [6,7]. Among these methods, adsorption is considered as the most prospective methods in wastewater treatment because of its economical and effective properties [8]. Various adsorbents have been developed for the removal of metal ions, and biosorbents receive the prior consideration of researchers due to their effective and eco-friendly properties.

Chitosan, a natural aminopolysaccharide, is mainly obtained from crustacean shells and fungal biomass [9]. Chitosan possesses outstanding adsorption

*Corresponding author.

capability at acidic environment toward heavy metal ions including Pb(II) because of its abundant amine and hydroxyl groups [10]. However, poor chemical stability and mechanical strength of chitosan at low pH value limit its application and make it difficult to be recovered and reused. Crosslinking is a useful method to improve the chemical stability and mechanical strength of chitosan [11]. However, the crosslinking reaction usually occurs at the hydroxyl and amine groups of chitosan, which are the active sites of adsorption. Thereby, the adsorption capacity decreases normally after crosslinking [12]. In addition, chitosan and its derivatives exhibit lower selectivity in the adsorption of metal ions. The selective adsorption can facilitate the recovery and reuse of metal ions, thus a selective biosorbent is favorable to the adsorption of metal ions. Ion-imprinting technology is an available method to enhance the adsorption performance and selectivity, and some evidences were found in previous literature. High selectivity and satisfactory adsorption capacity for the adsorption of Pb(II) were achieved with Pb(II)-imprinted polymer [13]. Pb (II)-imprinted crown ether showed higher capacity and selectivity than the non-imprinted crown ether [14]. Therefore, developing effective and selective biosorbents is proposed to be an important effort for the adsorption of heavy metal ions.

In the present work, an effective and selective ion-imprinted biosorbent was prepared from chitosan, using Pb(II) ions as templates and ethylene glycol diglycidyl ether (EGDE) as the crosslinker. The resultant Pb(II)-imprinted chitosan beads (Pb-ICB) were characterized by scanning electron microscopy (SEM), Fourier transform infrared spectrum (FTIR), X-ray diffraction (XRD), and Thermogravimetric analysis (TGA). The adsorption property and selectivity of Pb-ICB were evaluated for the adsorption of Pb(II). The adsorption kinetics was analyzed by the pseudo-first-order, pseudo-second-order kinetic, and intraparticle diffusion models. The Langmuir and Freundlich isotherm equations were used to assay the adsorption equilibrium, and the thermodynamic parameters were determined. Furthermore, the selectivity and reusability of Pb-ICB were investigated.

2. Experimental

2.1. Materials

Chitosan (Molecular weight: 1,000 kDa; Deacetylated degree: 85%) was purchased from Zhejiang aoxing biotechnology, China. EGDE was obtained from Tokyo chemical industry Co., Ltd, Japan. $Pb(NO_3)_2$ was provided by Tianjin Bodi chemical industry, China. Other chemicals were of analytical grade. Deionized water was used for the preparation of solutions throughout experiments.

2.2. Preparation of Pb-ICB

Chitosan (1.25 g) was dissolved completely in 50 mL acetic acid–sodium acetate buffer (pH 4.0, 0.2 mol/L) containing 50 mmol/L $Pb(NO_3)_2$. The chitosan solution was then added dropwise into 100 mL NaOH solution (2 mol/L) using a syringe needle with an inner diameter of 0.3 mm. After 10 h solidification, the resultant beads were collected and rinsed thoroughly with deionized water to pH 7.0, and transferred into 40 mL isopropyl-ketone solution (10% v/v). EGDE of 120 μL was added into the solution, and the solution was then incubated at 30℃ for 12 h in a shaker at 120 rpm for crosslinking. Afterward, the beads were placed into 5 mM EDTA-Na_2(pH 8.0) for 3 h with agitation to remove the Pb(II) templates. Finally, the beads were rinsed completely with deionized water and freeze-dried at −50℃. Non-imprinted chitosan beads (NICB) were prepared as the same procedure without the presence of $Pb(NO_3)_2$. The beads with the diameter of 1.0 mm were selected to perform the adsorption experiments.

2.3. Fourier transform infrared spectrum

FTIR is a powerful tool to detect the functional groups of compounds. FTIR was performed in the wave number range of 500–4,000 cm^{-1} on a KBr disk using a Tensor 27 Fourier transform infrared spectrometer (Bruker, Germany).

2.4. Scanning electron microscopy

The morphology of chitosan beads was observed using a NOVA NANO SEM 450 scanning electron microscope (FEI, USA).

2.5. X-ray diffraction

The XRD profiles of chitosan beads were recorded by a D8 Focus X-ray diffractometer (Bruker, Germany) with Cu Kα radiation.

2.6. Thermogravimetric analysis

TGA was performed with a HCT-2 thermogravimetric analyzer (HENGJIU instrument, China). Samples were heated from 30 to 600℃ at a rate of 10℃/min in N_2 atmosphere.

2.7. Adsorption experiments

The Pb(II) stock solution (1,000 mg/L) was prepared by dissolving $Pb(NO_3)_2$ in deionized water and diluted to the appropriate concentrations in the adsorption experiment. The adsorption experiment was conducted in a 250-mL flask with 50 mL Pb(II) solution, and the initial pH of the solution was adjusted to pH 4.5 with 0.1 mol/L HNO_3. Chitosan beads (0.15 g) were added into the Pb(II) solution, then the flask was incubated in a shaker at 120 rpm. The Pb(II) concentration was determined at intervals using an atomic adsorption spectrophotometer (thermo SOLAAR M6, USA). The adsorption capacity q_t (mg/g) was calculated according to Eq. (1).

$$q_t = \frac{(C_0 - C_t)V}{M} \tag{1}$$

where C_0 (mg/L) is the initial Pb(II) concentration; C_t (mg/L) is the Pb(II) concentration at time t; V (L) is the solution volume; W (g) is the mass of beads.

2.8. Selectivity experiments

To study the selectivity of Pb-ICB, the experiments on competitive adsorption were carried out by mixing Pb(II) and other metal ions at equal concentration. The distribution coefficient K_d (mL/g), selectivity coefficient $\beta_{Pb/M}$, and the relative selectivity coefficient β_r were defined as follows [15]:

$$K_d = \frac{q_e}{C_e} \tag{2}$$

$$\beta_{Pb/M} = \frac{K_{d(Pb)}}{K_{d(M)}} \tag{3}$$

$$\beta_r = \frac{\beta_{imprinted}}{\beta_{non\text{-}imprinted}} \tag{4}$$

where q_e (mg/g) is the equilibrium adsorption capacity; C_e (mg/L) is the equilibrium concentration of metal ions; $K_{d(Pb)}$ and $K_{d(M)}$ are the distribution coefficient of Pb(II) ions and other coexistent metal ions, respectively; $\beta_{imprinted}$ and $\beta_{non\text{-}imprinted}$ are the selectivity coefficients of the Pb-ICB and NICB, respectively.

2.9. Reusability of absorbents

The beads-loaded Pb(II) were recovered with 5 mM EDTA-Na_2 (pH 8.0) for 3 h, and then washed intensively with deionized water. The regenerated beads were used in the next adsorption cycle, and five cycles were carried out in this study.

3. Results and discussion

3.1. FTIR spectra

Fig. 1 shows the FTIR spectra of CTS, NICB, and Pb-ICB. Several typical adsorption bands were observed in the FTIR spectrum of original CTS. The locations and assignments of these bands were presented as follows: 3,441 cm^{-1} (the overlapping of N–H and O–H stretching vibration), 2,918 and 2,880 cm^{-1} (C–H stretching vibration of methyl and methylene), 1,653 cm^{-1} (C=O stretching vibration of amide I), 1,597 cm^{-1} (N–H bending vibration of amide II, $–NH_2$), 1,421 and 1,381 cm^{-1} (C–H bending vibration of methylene and the C–H symmetric stretching vibration of methyl, respectively), 1,325 cm^{-1} (C–N stretching vibration of amide III), 1,155 cm^{-1} (asymmetric stretching vibration of C–O–C), 1,088, and 1,034 cm^{-1} (C–O stretching vibration of C_3–OH and C_6–OH, respectively), 897 cm^{-1} (stretching vibration of saccharide ring) [16,17]. Compared with CTS, NICB showed some alterations in the FTIR spectrum due to the crosslinking reaction. The bands at 3,441 and 1,088 cm^{-1} shifted to low frequency at 3,433 and 1,072 cm^{-1}, respectively, and slight decrease in the band absorbance of $–NH_2$ was observed. These alterations indicate that the hydroxyl and amine groups of chitosan were involved in the crosslinking reaction. For Pb-ICB, the band of N–H and O–H stretching vibration shifted to 3,445 cm^{-1} and the band absorbance of $–NH_2$ decreased obviously, suggesting the involvement of the hydroxyl and amine groups in the imprinting reaction. In addition, the peak at 663 cm^{-1}, associated with the crystallinity [18],

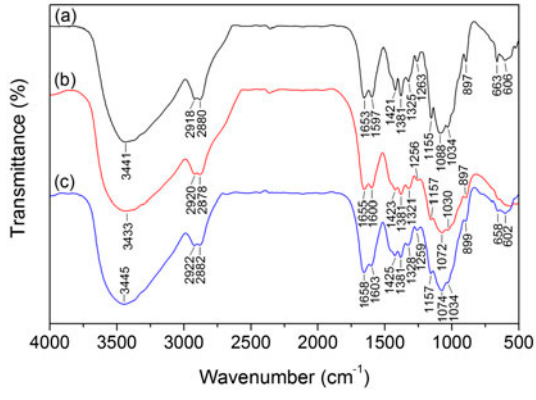

Fig. 1. FTIR spectra of CTS (a), NICB (b), and Pb-ICB (c).

appeared in CTS spectrum, but weakened dramatically in the spectra of NICB and Pb-ICB, which indicates the partial loss of the crystallinity of NICB and Pb-ICB.

3.2. Scanning electron microscopy

The SEM images of NICB and Pb-ICB are shown in Fig. 2. A large number of cavities were observed in Pb-ICB, whereas no obvious pore was found in NICB. The crosslinking reaction occurred at the hydroxyl and amine groups of chitosan. For Pb-ICB, the partial occupation of the hydroxyl and amine groups by Pb (II) ions led to the decrease in crosslinking sites. Therefore, Pb-ICB had lower crosslinking degree than NICB, which resulted in a flexible network of the matrix and a large number of cavities in Pb-ICB. The cavities in Pb-ICB increase the effective surface area and mass transfer efficiency, which can facilitate the adsorption of Pb(II) ions.

3.3. XRD patterns

The XRD patterns of CTS, NICB, and Pb-ICB are presented in Fig. 3. CTS showed two typical crystalline diffraction peaks at $2\theta = 10.8^\circ$ and $2\theta = 20.2^\circ$ assigned to crystal forms I and II, respectively [19]. These peaks were also observed in the spectra of NICB and Pb-ICB. However, the intensity of the peak at $2\theta = 10.8^\circ$ decreased, which indicates that the crosslinking and imprinting processes resulted in a partial loss of the crystallinity of chitosan.

Crystallinity plays an important role in the adsorption property of chitosan [20]. The crystalline regions of the polymer are not accessible to water and metal ions, whereas the metal ions penetrate easily through the amorphous structure. Therefore, the amorphous regions provide the access facilitation for the adsorption, enhancing the adsorption capacity. Pb-ICB exhibited lower intensity of the peak at $2\theta = 10.8^\circ$ than NICB, which reveals a comparably lower crystallinity of Pb-ICB. Accordingly, Pb-ICB had better adsorption performance than NICB.

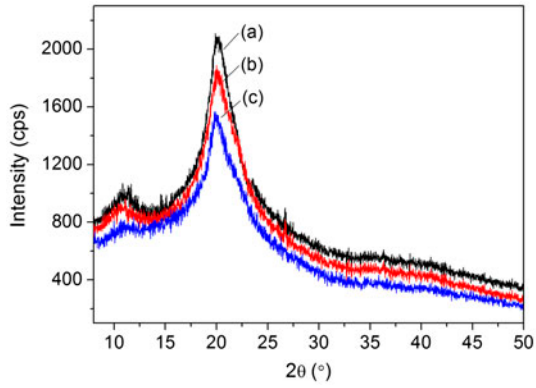

Fig. 3. XRD patterns of CTS (a), NICB (b), and Pb-ICB (c).

3.4. Thermogravimetric analysis

The thermogravimetric curves of CTS, NICB, and Pb-ICB are presented in Fig. 4. All tested samples showed two stages in weight loss, and the similar TGA curves were observed in the first stage for three samples. The first stage started from 60 and continued to 125°C with about 5–10% weight loss, which is attributed to the evaporation of residue water on the surface of the polymers [21]. The second stage, ascribed to the decomposition of polymers and the dehydration of saccharide rings [22], showed different patterns for three samples. For CTS, the initial decomposition temperature was observed at 268°C and the maximum decomposition rate occurred at 320°C. In contrast, the decomposition of Pb-ICB started at 226°C and reached the maximum rate at 307°C; the decomposition of NICB started at 234°C and reached the maximum rate at 310°C. These changes in the decomposition temperatures suggest that NICB and

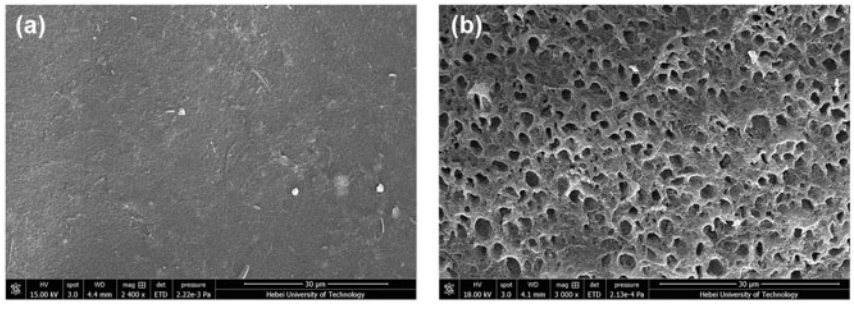

Fig. 2. SEM micrographs of NICB (a) and Pb-ICB (b).

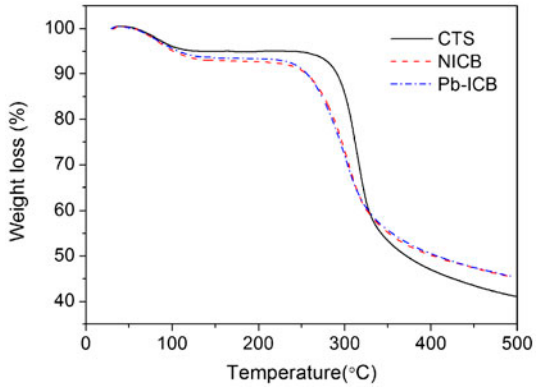

Fig. 4. Thermogravimetric curves of CTS, NICB, and Pb-ICB.

Pb-ICB had lower thermal stability than CTS. The thermogravimetric property relates to the crystallinity, and it illustrates the change of physicochemical structure of the polymer. Low thermal stability of NICB and Pb-ICB was mainly due to the breakage of hydrogen bonds in the crystalline regions by crosslinking. The breakage of hydrogen bonds results in the increase in free amine and hydroxyl groups, which can facilitate the adsorption. Moreover, thermal stability was found to be slightly lower for Pb-ICB relative to NICB, suggesting that Pb-ICB had a higher adsorption capacity than NICB.

3.5. Adsorption kinetics

The time dependence of adsorption capacities of Pb(II) onto NICB and Pb-ICB are shown in Fig. 5. The adsorption capacities of Pb(II) increased rapidly within the first 50 min, and then gradually reached the equilibrium beyond 130 min. The high initial adsorption rate is ascribed to the sufficient adsorption sites available, strong chelation, and the effective mass transfer [14]. Moreover, Pb-ICB exhibited a higher adsorption capacity than NICB due to its better affinity and internal mass transfer.

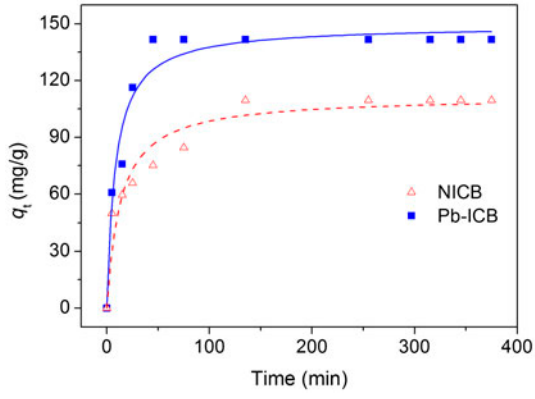

Fig. 5. Adsorption kinetics for the adsorption of Pb(II) onto NICB and Pb-ICB.

Kinetics analysis is a crucial work in the adsorption investigation because it can reveal the mechanism and rate-limiting step of the adsorption process. Herein, the pseudo-first-order kinetic model, pseudo-second-order kinetic model, and intraparticle diffusion model were applied to analyze the experimental data. The linear form of pseudo-first-order model [23] is usually expressed as Eq. (5).

$$\ln(q_e - q_t) = \ln q_e - k_1 t \tag{5}$$

where q_e (mg/g) is the equilibrium adsorption capacity; q_t (mg/g) is the adsorption capacity time t (min); k_1 (min^{-1}) is the rate constant of pseudo-first-order model.

The linear fitting curves of $\ln(q_e - q_t)$ vs. t were plotted from the experimental data. The model parameters q_e and k_1 were determined by the intercepts and slopes of the plots, respectively. Low correlation coefficients R^2 (0.9342 for Pb-ICB and 0.8220 for NICB) were obtained for pseudo-first-order model (Table 1) and large discrepancies between the calculated adsorption capacities ($q_{e,cal}$) and the experimental adsorption capacities ($q_{e,exp}$) were observed. These results suggest that the adsorption process of Pb(II) did not follow the pseudo-first-order model.

The linear form of pseudo-second-order kinetic model [24] is expressed as follows:

$$\frac{t}{q_t} = \frac{1}{k_2 q_e^2} + \frac{t}{q_e} \tag{6}$$

where k_2 (g/(mg min)) is the rate constant of pseudo-second-order model.

The linear fitting plots of t/q_t vs. t are shown in Fig. 6, and the parameters were summarized in Table 1. High correlation coefficients (0.9994 for Pb-ICB and 0.9980 for NICB) were achieved for pseudo-second-order model and the values of $q_{e,cal}$ were very close to that of $q_{e,exp}$, which showed that the adsorption processes of Pb(II) onto NICB and Pb-ICB well fitted the pseudo-second-order model. These results indicate that the adsorption process of Pb(II) was a chemical reaction through sharing or exchange of electrons between chitosan and Pb(II), and the chemisorption was the rate-limiting step controlling the adsorption process. Moreover, higher values of k_2 and $q_{e,cal}$ were obtained for Pb-ICB

Table 1
Kinetic parameters for the adsorption of Pb(II) onto Pb-ICB and NICB

		First-order kinetic model			Second-order kinetic model			Intraparticle diffusion model	
Adsorbents	$q_{e,exp}$ (mg/g)	$q_{e,cal}$ (mg/g)	k_1 (1/min)	R^2	$q_{e,cal}$ (mg/g)	k_2 (g/(mg min))	R^2	k_i (mg/(g $min^{1/2}$))	R^2
NICB	109.59	75.04	0.01619	0.8220	114.94	0.56×10^{-3}	0.9980	8.9080	0.8570
Pb-ICB	141.69	133.62	0.06256	0.9342	144.30	1.25×10^{-3}	0.9994	21.8425	0.9655

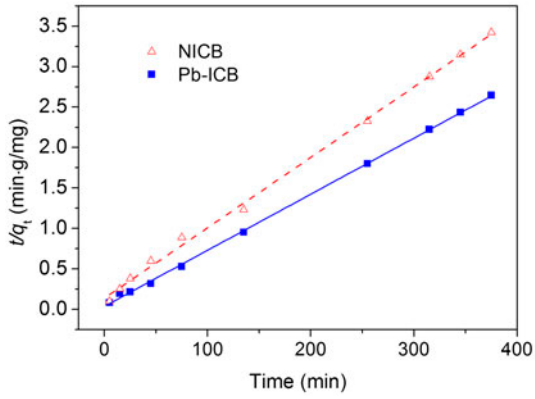

Fig. 6. Pseudo-second-order kinetic plots for the adsorption of Pb(II) onto NICB and Pb-ICB.

relative to NICB, demonstrating that the imprinting enhanced the adsorption rate and performance of chitosan beads.

The adsorption process of adsorbate onto a porous adsorbent in aqueous solutions involved several steps, including bulk diffusion, film diffusion, and intraparticle diffusion. Generally, the bulk diffusion and film diffusion are sufficiently rapid and not rate-determining factors, whereas the intraparticle diffusion is considered as the rate-limiting step in a well-stirred system [25]. Therefore, we further analyzed the adsorption process with intraparticle diffusion model [26] expressed as Eq. (7).

$$q_t = k_i t^{1/2} + C \tag{7}$$

where k_i (mg/(g $min^{1/2}$)) is the rate constant of intraparticle diffusion; C (mg/g) is the thickness of the boundary layer.

The fitting plots are shown in Fig. 7, and the calculated parameters are listed in Table 1. The plots showed two portions, a linear slope and a plateau, which revealed that two stages occurred during the adsorption process. The slope portion represents the intraparticle diffusion stage, and the plateau portion corresponds to the equilibrium stage [25]. The diffusion constant k_i was found to be higher for Pb-ICB relative to NICB, which demonstrated that Pb-ICB had low diffusion resistance than NICB due to its cavity structure.

3.6. Adsorption isotherm

Adsorption isotherm is invaluable in understanding an adsorption process because its physicochemical parameters provide an insight into the adsorption mechanism, the surface properties and the affinity degree of adsorbent [27]. In the present study, Langmuir and Freundlich isotherms were used to describe the adsorption equilibrium of Pb(II) onto NICB and Pb-ICB. The Langmuir isotherm generally expresses the monolayer adsorption on an energetically homogeneous surface [28], whereas Freundlich isotherm is an empirical equation and usually used to describe the multilayer adsorption on an energetically heterogeneous surface [29]. The Langmuir and Freundlich isotherms are expressed as Eqs. (8) and (9), respectively.

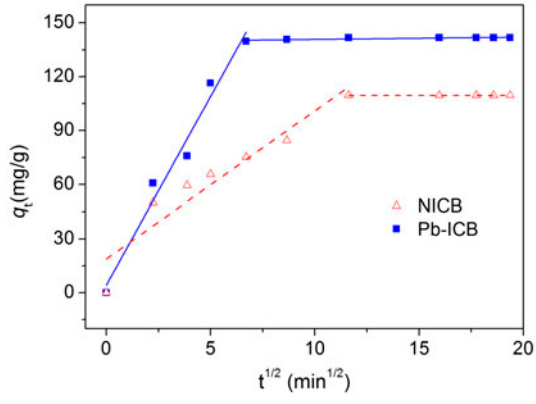

Fig. 7. Intraparticle diffusion kinetic plots for the adsorption of Pb(II) onto NICB and Pb-ICB.

$$\frac{C_e}{q_e} = \frac{1}{b\,q_m} + \frac{C_e}{q_m} \quad (8)$$

$$\ln q_e = \ln K_F + \frac{1}{n}\ln C_e \quad (9)$$

where C_e (mg/L) is the equilibrium concentration of Pb(II); q_m (mg/g) is the theoretical maximum adsorption capacity; b (L/g) is the Langmuir adsorption constant; K_F (mg/g) is the Freundlich isotherm constant related to the maximum adsorption capacity; n is the heterogeneity factor.

The adsorption isotherm experiments were conducted at 293, 303, and 313 K, and the calculated parameters of Langmuir and Freundlich isotherms are given in Table 2. Based on the correlation coefficients (R^2), the adsorption of Pb(II) onto NICB, and Pb-ICB fitted Langmuir isotherm better than Freundlich isotherm, indicating that the determining interaction between chitosan and Pb(II) was the chemisorption and the distribution of active sites on the surface of NICB and Pb-ICB was homogeneous. Langmuir constants (b), related to the affinity of active sites, were found to be higher for Pb-ICB relative to NICB, which demonstrates that Pb-ICB possessed better affinity to Pb(II) ions than NICB. Moreover, the maximum adsorption capacity (q_m) of Pb-ICB, reached 177.62 mg/g at 303 K, was comparably higher than those of NICB and other chitosan-based biosorbents recently reported [14,30]. In addition, for Freundlich isotherm, the constant (n) values were more than 1.0, which means that the adsorption intensity was favorable at high concentration.

3.7. Adsorption thermodynamics

The thermodynamic parameters including standard Gibbs free energy change ΔG° (kJ/mol), standard enthalpy change ΔH° (kJ/mol), and standard entropy change ΔS° (J/mol K) were calculated from Langmuir constant (K_L) according to the follows [31]:

$$\Delta G^\circ = -RT\ln K_L \quad (10)$$

$$\ln K_L = \frac{\Delta S^\circ}{R} - \frac{\Delta H^\circ}{RT} \quad (11)$$

where K_L (L/mol) is the Langmuir constant, which was obtained by multiplying the constant b (Table 2) with the molar weight of lead; T (K) is the temperature; R is the gas constant (8.314 J/K mol).

The linear fitting plots of $\ln K_L$ vs. $1/T$ were obtained from the above Langmuir constants, and the ΔH° and ΔS° were calculated from the slope and intercept of the plots, respectively. The calculated values of ΔG°, ΔH°, and ΔS° are presented in Table 3. The negative values of ΔG° showed that the adsorption of Pb (II) onto NICB and Pb-ICB occurred spontaneously; the decrease in ΔG° with the increase in temperature implied that the adsorption process was more favorable at higher temperature. The positive values of ΔH° showed that the adsorption process was endothermic in nature, and the positive ΔS° indicated that the disorder of the system increased during the adsorption process. The values of $|T\Delta S^\circ|$ were greater than that of $|\Delta H^\circ|$, which suggests that the adsorption was dominated by entropy rather than enthalpy change [32]. Moreover, higher entropy value of Pb-ICB revealed also that Pb-ICB possessed better affinity toward Pb(II) ions than NICB.

3.8. Selectivity of Pb-ICB

To investigate the selectivity of Pb-ICB, we conducted the experiments using the binary system of Pb (II) with other ions. The distribution coefficient (K_d), selectivity coefficient ($\beta_{Pb/M}$), and relative selectivity coefficient (β_r) are listed in Table 4. Compared with

Table 2
Isotherm constants for the adsorption of Pb(II) onto NICB and Pb-ICB

		Langmuir constants			Freundlich constants		
Adsorbents	T (K)	b (L/g)	q_m (mg/g)	R^2	K_F (mg/g)	n	R^2
NICB	293	5.933	125.79	0.9991	110.218	3.008	0.9552
	303	6.930	125.47	0.9933	109.292	4.152	0.9879
	313	8.442	123.46	0.9993	114.228	3.331	0.9568
Pb-ICB	293	7.194	168.35	0.9977	149.089	3.745	0.9787
	303	10.568	177.62	0.9932	162.593	5.483	0.8988
	313	11.104	176.06	0.9987	164.633	4.296	0.9695

Table 3
Thermodynamic constants for the adsorption of Pb(II) onto Pb-ICB and NICB

Adsorbents	T (K)	K_L (L/mol)	ΔG° (kJ/mol)	ΔH° (kJ/mol)	ΔS° (J/(K mol))
NICB	293	1.229×10^3	−17.33	13.43	104.90
	303	1.436×10^3	−18.31		
	313	1.749×10^3	−19.43		
Pb-ICB	293	1.491×10^3	−17.80	16.68	118.10
	303	2.189×10^3	−19.38		
	313	2.301×10^3	−20.14		

Table 4
Selectivity of Pb-ICB and NICB in binary metal system

		NICB		Pb-ICB		
Binary system	Ions	K_d (mL/g)	$\beta_{Pb/M}$	K_d (mL/g)	$\beta_{Pb/M}$	β_r
Pb-Cu	Pb	68.745		265.486		
	Cu	71.062	0.967	171.321	1.550	1.603
Pb-Cd	Pb	74.909		251.254		
	Cd	64.309	1.165	118.707	2.117	1.817

NICB, Pb-ICB showed higher values of K_d and $\beta_{Pb/M}$, which demonstrates that the imprinting enhanced the adsorption capacity and selectivity of Pb-ICB. After imprinting, the specific surface area and active sites increased due to the cavity structure created in Pb-ICB, and the matrix network of Pb-ICB was coordinated to Pb(II) ions in size, shape, and geometry. Therefore, Pb-ICB exhibited better adsorption capacity and selectivity than NICB. Moreover, it was found that the relative selectivity coefficient (β_r) of Pb-ICB to Pb(II) was higher in the Pb-Cd system than that in the Pb-Cu system. The adsorption performance of the adsorbent varies with the species of metal ions. The coordinative abilities of metal ions with adsorbents can be identified using the theory of hard and soft acids and bases [33]. When forming coordinative bonds, the metal ions prefer the ligands of the same kind to those of different kinds [20]. Cu(II) and Pb(II) are borderline acids, whereas Cd (II) is a soft acid. The coordination of Cu(II) and Pb(II) with chitosan is priority to Cd(II) because the ligands in chitosan are hard bases, which indicates that the effect of Cu(II) on the adsorption of Pb(II) is greater than that of Cd(II). Therefore, the relative selectivity of Pb-ICB to Pb(II) was better in the Pb-Cd system than that in the Pb-Cu system.

3.9. Reusability of Pb-ICB

To study the reusability of the adsorbent, we conducted the adsorption–desorption in five cycles and the results are shown in Fig. 8. The adsorption capacities of NICB and Pb-ICB decreased with the increase in reuse times, which may be because of the damage to the specific geometry structure and the loss of active sites by the repeated adsorption–desorption processes [34]. After five cycles, the adsorption capacities of NICB and Pb-ICB decreased by 33.71 and 32.42%, respectively, which showed that both NICB and Pb-ICB possessed good reusability within five cycles of adsorption–desorption.

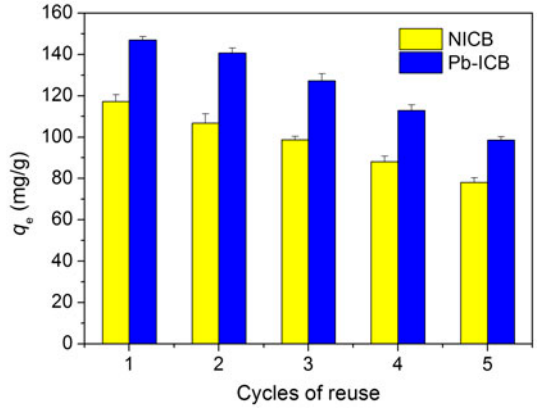

Fig. 8. Reusability of NICB and Pb-ICB.

4. Conclusions

In the present study, Pb-ICB were prepared using Pb(II) ions as templates to improve the adsorption capacity and selectivity. The resultant Pb-ICB showed more cavities, but less crystallinity and thermal stability than NICB. The enhanced and selective adsorption of Pb(II) ions onto Pb-ICB was achieved, and Pb-ICB exhibited good reusability within five cycles of reuse. Our results suggest that Pb-ICB possessed excellent adsorption performance and had potential to become a novel biosorbent with effective and selective properties.

Acknowledgments

This work was supported by the Scientific Research Foundation for the Returned Overseas Chinese Scholars, Department of Human Resources and Social Security of Hebei Province, China.

References

[1] D. Chauhan, N. Sankararamakrishnan, Highly enhanced adsorption for decontamination of lead ions from battery wastewaters using chitosan functionalized with xanthate, Bioresour. Technol. 99 (2008) 9021–9024.
[2] M.A.P. Cechinel, S.M.A.G. Ulson de Souza, A.A. Ulson de Souza, Study of lead(II) adsorption onto activated carbon originating from cow bone, J. Cleaner Prod. 65 (2014) 342–349.
[3] Ö. Gerçel, H.F. Gerçel, Adsorption of lead(II) ions from aqueous solutions by activated carbon prepared from biomass plant material of *Euphorbia rigida*, Chem. Eng. J. 132 (2007) 289–297.
[4] R. Dongre, M. Thakur, D. Ghugal, J. Meshram, Bromine pretreated chitosan for adsorption of lead(II) from water, Bull. Mater. Sci. 35 (2012) 875–884.
[5] T. Liu, X. Yang, Z.L. Wang, X. Yan, Enhanced chitosan beads-supported Fe^0-nanoparticles for removal of heavy metals from electroplating wastewater in permeable reactive barriers, Water Res. 47 (2013) 6691–6700.
[6] M. Suguna, N.S. Kumar, V. Sreenivasulu, A. Krishnaiah, Removal of Pb(II) from aqueous solutions by using chitosan coated zero valent iron nanoparticles, Sep. Sci. Technol. 49 (2014) 1613–1622.
[7] N. Unlu, M. Ersoz, Adsorption characteristics of heavy metal ions onto a low cost biopolymeric sorbent from aqueous solutions, J. Hazard. Mater. 136 (2006) 272–280.
[8] W.S. Wan Ngah, C.S. Endud, R. Mayanar, Removal of copper(II) ions from aqueous solution onto chitosan and cross-linked chitosan beads, React. Funct. Polym. 50 (2002) 181–190.
[9] H.A. Shawky, Synthesis of ion-imprinting chitosan/PVA crosslinked membrane for selective removal of Ag(I), J. Appl. Polym. Sci. 114 (2009) 2608–2615.
[10] G.Z. Kyzas, D.N. Bikiaris, E.A. Deliyanni, Advanced low-swelling chitosan/graphite oxide-based biosorbents, Mater. Lett. 128 (2014) 46–49.
[11] C.Y. Chen, C.Y. Yang, A.H. Chen, Biosorption of Cu(II), Zn(II), Ni(II) and Pb(II) ions by cross-linked metal-imprinted chitosans with epichlorohydrin, J. Environ. Manage. 92 (2011) 796–802.
[12] E.S. Dragan, A.I. Cocarta, M.V. Dinu, Facile fabrication of chitosan/poly(vinyl amine) composite beads with enhanced sorption of Cu^{2+}. Equilibrium, kinetics, and thermodynamics, Chem. Eng. J. 255 (2014) 659–669.
[13] Y. Liu, Z. Liu, J. Gao, J. Dai, J. Han, Y. Wang, J. Xie, Y. Yan, Selective adsorption behavior of Pb(II) by mesoporous silica SBA-15-supported Pb(II)-imprinted polymer based on surface molecularly imprinting technique, J. Hazard. Mater. 186 (2011) 197–205.
[14] X. Luo, L. Liu, F. Deng, S. Luo, Novel ion-imprinted polymer using crown ether as a functional monomer for selective removal of Pb(II) ions in real environmental water samples, J. Mater. Chem. A 1 (2013) 8280.
[15] Y. Ren, M. Zhang, D. Zhao, Synthesis and properties of magnetic Cu(II) ion imprinted composite adsorbent for selective removal of copper, Desalination 228 (2008) 135–149.
[16] D.H.K. Reddy, S.M. Lee, Synthesis and characterization of a chitosan ligand for the removal of copper from aqueous media, J. Appl. Polym. Sci. 130 (2013) 4542–4550.
[17] F. Brunel, N.E. El Gueddari, B.M. Moerschbacher, Complexation of copper(II) with chitosan nanogels: Toward control of microbial growth, Carbohydr. Polym. 92 (2013) 1348–1356.
[18] S. Mima, M. Miya, R. Iwamoto, S. Yoshikawa, Highly deacetylated chitosan and its properties, J. Appl. Polym. Sci. 28 (1983) 1909–1917.
[19] Z. Yalinca, E. Yilmaz, F.T. Bullici, Evaluation of chitosan tripolyphosphate gel beads as bioadsorbents for iron in aqueous solution and in human blood *in vitro*, J. Appl. Polym. Sci. 125 (2012) 1493–1505.
[20] E. Guibal, Interactions of metal ions with chitosan-based sorbents: A review, Sep. Purif. Technol. 38 (2004) 43–74.
[21] R. Laus, V.T. de Fávere, Competitive adsorption of Cu(II) and Cd(II) ions by chitosan crosslinked with epichlorohydrin–triphosphate, Bioresour. Technol. 102 (2011) 8769–8776.
[22] C. Stefanescu, W.H. Daly, I.I. Negulescu, Biocomposite films prepared from ionic liquid solutions of chitosan and cellulose, Carbohydr. Polym. 87 (2012) 435–443.
[23] Y.-S. Ho, G. McKay, Sorption of dye from aqueous solution by peat, Chem. Eng. J. 70 (1998) 115–124.
[24] Y.-S. Ho, G. McKay, Pseudo-second order model for sorption processes, Process Biochem. 34 (1999) 451–465.
[25] W.S. Ngah, S. Fatinathan, Adsorption characterization of Pb(II) and Cu(II) ions onto chitosan-tripolyphosphate beads: Kinetic, equilibrium and thermodynamic studies, J. Environ. Manage. 91 (2010) 958–969.
[26] S.K. Singh, T.G. Townsend, D. Mazyck, T.H. Boyer, Equilibrium and intra-particle diffusion of stabilized landfill leachate onto micro- and meso-porous activated carbon, Water Res. 46 (2012) 491–499.
[27] K.Y. Foo, B.H. Hameed, Insights into the modeling of adsorption isotherm systems, Chem. Eng. J. 156 (2010) 2–10.

[28] Y. Lu, J. He, G. Luo, An improved synthesis of chitosan bead for Pb(II) adsorption, Chem. Eng. J. 226 (2013) 271–278.
[29] X. Lan, P. Liang, Y. Yang, Adsorption of tartaric acid–cadmium complex by imprinted chitosan biopolymer, Desalin. Water Treat. 51 (2013) 3883–3888.
[30] W. Jiang, H. Su, H. Huo, T. Tan, Synthesis and properties of surface molecular imprinting adsorbent for removal of Pb^{2+}, Appl. Biochem. Biotechnol. 160 (2010) 467–476.
[31] H. Yan, J. Dai, Z. Yang, H. Yang, R. Cheng, Enhanced and selective adsorption of copper(II) ions on surface carboxymethylated chitosan hydrogel beads, Chem. Eng. J. 174 (2011) 586–594.
[32] H. Li, S. Bi, L. Liu, W. Dong, X. Wang, Separation and accumulation of Cu(II), Zn(II) and Cr(VI) from aqueous solution by magnetic chitosan modified with diethylenetriamine, Desalination 278 (2011) 397–404.
[33] R.G. Pearson, Hard and soft acids and bases, J. Am. Chem. Soc. 85 (1963) 3533–3539.
[34] S. Yang, Y. Wang, M. Xu, M. He, M. Zhang, D. Ran, X. Jia, Synthesis of modified chitosan-based molecularly imprinted polymers for adsorptive protein separation, Anal. Methods 5 (2013) 5471–5477.